Interdiffusion process in lattice-matched $In_xGa_{1-x}As_yP_{1-y}$/InP and GaAs/$Al_xGa_{1-x}As$ quantum wells

Kohki Mukai, Mitsuru Sugawara, and Susumu Yamazaki
Fujitsu Laboratories Ltd., 10-1 Morinosato-Wakamiya, Atsugi 243-01, Japan
(Received 13 May 1993)

We derive a formula that describes interdiffusion profiles of quantum wells and shows how the formula accurately models interdiffusion in quantum wells of lattice-matched $In_xGa_{1-x}As_yP_{1-y}$ and $Al_xGa_{1-x}As$ alloy semiconductors. Our formula includes the different interdiffusion coefficients between layers and interfacial discontinuity of interdiffused species. Our formula explains how quantum energy shifts due to interdiffusion vary with annealing time and annealing temperature in various wide well layers of both $In_xGa_{1-x}As_yP_{1-y}$/InP and GaAs/$Al_xGa_{1-x}As$ quantum wells. We also show the quantitative difference between interdiffusion profiles of these two materials.

I. INTRODUCTION

Quantum wells composed of III-V compound semiconductors have a wide range of optical and electronic applications. It is difficult to study interdiffusion in the quantum wells, however, because of their small size and other characteristics of the material. Since well layers are several nanometers wide, the interdiffusion profiles cannot be measured directly. The profiles in quantum wells are not necessarily the same as those measured directly in wider heterostructures. Interdiffusion causes lattice strain in III-V compound semiconductors. When the layer widths exceed the elastic limit, the lattice strain induces dislocations that affect the interdiffusion process. Since the well layers are thin, interdiffusion penetrates alternate barrier layers, which further complicates the interdiffusion profiles. The interdiffusion of group-III atoms and of group-V atoms must be considered separately, since the atoms do not mix because of their polarities.

Interdiffusion of GaAs/$Al_xGa_{1-x}As$ quantum wells has been heavily studied. Group-III atoms are the only possible interdiffusion species and are known to begin interdiffusing above 800 °C.[1] The influence of implanting active impurities[2-8] and lattice defects[9-12] on interdiffusion was studied by using transmission electron microscopy or measuring quantum energy shifts. The interdiffused compositional profile of these materials was first reported by Chang and Koma[1] for 150-nm-wide GaAs/AlAs double heterostructures using Auger electron spectroscopy. The profiles were error functional and symmetrical. Considering that the strain in interdiffused $Al_xGa_{1-x}As$ layers is negligible, several other researchers used Chang and Koma's profiles to explain how quantum energy shifts in GaAs/$Al_xGa_{1-x}As$ quantum wells relate to interdiffusion.[12-14] These researchers did not, however, directly examine or further confirm the interdiffusion profile of the quantum wells.

After GaAs/$Al_xGa_{1-x}As$ quantum wells, the next most heavily studied structure is $In_xGa_{1-x}As_yP_{1-y}$/InP quantum wells, which are the main components of the 1-μm-region optoelectronic devices. This system has two possible interdiffusion species, group-III atoms and group-V atoms. Group-V atoms reportedly interdiffuse more easily than group-III atoms.[15] Arsenic and phosphorus atoms begin to interdiffuse at about 500 °C.[16] The influence of impurities and defects on interdiffusion properties has been studied,[17-23] but the interdiffusion profile in $In_xGa_{1-x}As_yP_{1-y}$/InP quantum wells is not well understood. The interdiffusion profile cannot be estimated by direct observation of wide heterostructures since the lattice constant of $In_xGa_{1-x}As_yP_{1-y}$ materials strongly depends on the composition. Some researchers have pointed out the difference between interdiffusion profiles of $In_{0.53}Ga_{0.47}As$/InP quantum wells and those of GaAs/$Al_xGa_{1-x}As$ systems using indirect methods. Nakashima *et al.*[15] used x-ray analysis and the Fleming model[24] to show that arsenic composition in an $In_{0.53}Ga_{0.47}As$ well layer evenly decreases and that the interdiffused arsenic atoms stagnate near the interface of an InP barrier layer side. Fujii *et al.*[16] reported that there must be a large compositional discontinuity of group-V atoms at an interface, even after interdiffusion, by roughly estimating the dependence of quantum energy shifts on the well-layer width.

In this paper, we present a formula that comprehensively describes interdiffusion profiles in quantum wells and evaluate the interdiffusion process of group-V atoms in lattice-matched $In_xGa_{1-x}As_yP_{1-y}$/InP and that of group-III atoms in GaAs/$Al_xGa_{1-x}As$ quantum wells with the formula. We derive our formula by analytically solving diffusion equations for a piled three-layer system, taking into account the different interdiffusion coefficients between layers and the compositional discontinuity of diffused species at interfaces. We relate our formula to the dependence of quantum energy shifts on annealing time and annealing temperature for various wide well layers. We show that the dependence of quantum energy shifts is very different for $In_xGa_{1-x}As_yP_{1-y}$/InP and GaAs/$Al_xGa_{1-x}As$ quantum wells and that our formula explains the difference.

II. MODEL OF THE INTERDIFFUSION PROFILE

We solved the linear diffusion equations for a piled three-layer structure. In our mathematical model, the outside layer extends infinitely in the $-x$ and $+x$ directions. We defined the origin of the x axis as the center of the middle layer. There are two boundaries, at $x=-L$ and $x=L$. First, we solved linear diffusion equations assuming a momentary plane source at $x=\xi$. We then integrated the solutions, using an initial composition profile, to fit the actual structure. In the actual structure, diffusion species in the two outside layers can mix via the middle layer, equivalent to a single quantum well. To find a solution, we made two generalizing assumptions.[25] First, we assumed that the diffusion coefficients of outside layers and middle layer are different, and that the outside layers have a common diffusion coefficient. Second, we assumed a certain distribution ratio for diffused species at the interface,[26] so the composition species can be discontinuous at the interface. We made two more assumptions to eliminate difficulties in solving the diffusion equations: (i) both the interdiffusion coefficient in each layer and the distribution ratio at the interface are constant during interdiffusion; (ii) we ignored the Smigelskas-Kirkendall effect, where unbalanced velocity of interdiffusion causes the interface to move. We show in Sec. V that practical results are consistent with these assumptions. In addition, when the thicknesses of layers are smaller than 30 Å, a gradient correction term should be considered.[27] In this work, we neglected the correction term.

We derived our formula as shown below. The three linear diffusion equations are

$$\frac{\partial C_1(x,t)}{\partial t}=D_1\frac{\partial^2 C_1(x,t)}{\partial x^2},\quad t\geq 0,\ x\geq L \tag{1}$$

$$\frac{\partial C_2(x,t)}{\partial t}=D_2\frac{\partial^2 C_2(x,t)}{\partial x^2},\quad t\geq 0,\ |x|<L \tag{2}$$

and

$$\frac{\partial C_3(x,t)}{\partial t}=D_1\frac{\partial^2 C_3(x,t)}{\partial x^2},\quad t\geq 0,\ x\leq -L\ . \tag{3}$$

The boundary conditions are

$$C_1(x,t)=kC_2(x,t)\ \text{ for } x\rightarrow L\ , \tag{4}$$

$$C_3(x,t)=kC_2(x,t)\ \text{ for } x\rightarrow -L\ , \tag{5}$$

$$D_1\frac{\partial C_1(x,t)}{\partial x}=D_2\frac{\partial C_2(x,t)}{\partial x}\ \text{ for } x\rightarrow L\ , \tag{6}$$

$$D_1\frac{\partial C_3(x,t)}{\partial x}=D_2\frac{\partial C_2(x,t)}{\partial x}\ \text{ for } x\rightarrow -L \tag{7}$$

and the initial conditions are

$$C_1(x,t)=\delta(x-\xi),\quad C_2(x,t)=C_3(x,t)=0 \quad \text{for } t\rightarrow 0\ . \tag{8}$$

Here C_i $(i=1,3)$ is the concentration of diffusion species in the outside layers and C_2 is the concentration in the middle layer. D_i $(i=1,2)$ is the diffusion coefficient in the outside layers and the middle layer, respectively. The interfacial distribution ratio of concentration is $k=C_i/C_2$ $(i=1,3)$. Equations (4) and (5) model the discontinuous concentration at interfaces, while Eqs. (6) and (7) express flux continuity. $\delta(x-\xi)$ is a delta function.

We solved these diffusion equations and obtained the following (see the Appendix):

$$C_1(x,t)=\frac{1}{2\sqrt{\pi D_1 t}}\left[\exp\left\{-\frac{(x-\xi)^2}{4D_1 t}\right\}-\frac{1-ak}{1+ak}\exp\left\{-\frac{(x-2L+\xi)^2}{4D_1 t}\right\}+\frac{4ak}{(1+ak)^2}\sum_{n=1}^{\infty}\left[\frac{1-ak}{1+ak}\right]^{2n-1}\exp\left\{-\frac{(x-2L+4aL+\xi)^2}{4D_1 t}\right\}\right],\quad x\geq L \tag{9}$$

$$C_2(x,t)=\frac{1}{2\sqrt{\pi D_1 t}}\frac{2a}{1+ak}\sum_{n=1}^{\infty}\left[\frac{1-ak}{1+ak}\right]^{2(n-1)}\left[\exp\left[-\frac{\left\{x+\frac{L}{a}-(4n-3)L-\frac{\xi}{a}\right\}^2}{4D_2 t}\right]+\frac{1-ak}{1+ak}\exp\left[-\frac{\left\{x-\frac{L}{a}-(4n-1)L+\frac{\xi}{a}\right\}^2}{4D_2 t}\right]\right],\quad |x|<L \tag{10}$$

$$C_3(x,t)=\frac{1}{2\sqrt{\pi D_1 t}}\frac{4ak}{(1+ak)^2}\sum_{n=1}^{\infty}\left[\frac{1-ak}{1+ak}\right]^{2(n-1)}\exp\left[-\frac{\left\{x+2L-(4n-2)aL-\xi\right\}^2}{4D_1 t}\right],\quad x\leq -L\ , \tag{11}$$

where $a=\sqrt{D_1/D_2}$.

We next integrated Eqs. (9)–(11) using the initial composition profile. We used the initial conditions

$$F(x,0)=F_0, \quad |x|\geq L \tag{12}$$

$$F(x,0)=0, \quad |x|<L \tag{13}$$

and calculated

$$F(x,t)=F_0\left[\int_L^{\infty}C_1(x,t)d\xi+\int_{-\infty}^{-L}C_3(-x,t)d\xi\right], \quad x\geq L \tag{14}$$

$$F(x,t)=F_0\left[\int_L^{\infty}C_2(x,t)d\xi+\int_{-\infty}^{-L}C_2(-x,t)d\xi\right], \quad |x|<L \tag{15}$$

$$F(x,t)=F_0\left[\int_L^{\infty}C_3(x,t)d\xi+\int_{-\infty}^{-L}C_1(-x,t)d\xi\right], \quad x\leq -L\ . \tag{16}$$

We then obtained the formulas

$$F(x,t)=\frac{F_0}{2}\left[1+\mathrm{erf}\left[\frac{|x|-L}{2\sqrt{D_1 t}}\right]-\frac{1-ak}{1+ak}\left\{1-\mathrm{erf}\left[\frac{|x|-L}{2\sqrt{D_1 t}}\right]\right\}+\frac{4ak}{(1+ak)^2}\sum_{n=1}^{\infty}\left[\frac{1-ak}{1+ak}\right]^{2(n-1)}\left[1-\mathrm{erf}[|x|-L+(4n-2)aL]+\frac{1-ak}{1+ak}\left\{1-\mathrm{erf}\left[\frac{|x|-L+4naL}{2\sqrt{D_{1t}}}\right]\right\}\right]\right], \quad |x|\geq L \tag{17}$$

$$F(x,t)=\frac{F_0 a}{1+ak}\sum_{n=1}^{\infty}\left[\frac{1-ak}{1+ak}\right]^{2(n-1)}\left[2+\mathrm{erf}\left[\frac{x-(4n-3)L}{2\sqrt{D_2 t}}\right]-\mathrm{erf}\left[\frac{x+(4n-3)L}{2\sqrt{D_2 t}}\right]+\frac{1-ak}{1+ak}\left\{2-\mathrm{erf}\left[\frac{x+(4n-3)L}{2\sqrt{D_2 t}}\right]+\mathrm{erf}\left[\frac{x-(4n-1)L}{2\sqrt{D_2 t}}\right]\right\}\right], \quad |x|<L\ . \tag{18}$$

Equations (17) and (18) generally give the concentrations of diffused species; these equations describe the interdiffusion profile when $F(x,t)$ is regarded as the composition of layers. In a practical analysis of interdiffusion in quantum wells, we determine three unknown material specific parameters D_1 (in barrier layer), D_2 (in well layer), and k in this formula.

III. EXPERIMENT

We grew experimental samples by metalorganic vapor-phase epitaxy. Samples were undoped $In_{0.53}Ga_{0.47}As/InP$ and

$$In_{0.53}Ga_{0.47}As/In_{0.70}Ga_{0.30}As_{0.61}P_{0.39}$$

single quantum wells (SQW's) on (001) InP substrates grown at 570 °C and undoped $GaAs/Al_{0.25}Ga_{0.75}As$ SQW's on (001) GaAs substrates grown at 720 °C. Each sample had a cap layer, quantum-well layers, and a buffer layer on the substrate. Quantum-well layers were composed of four well layers with different thicknesses to give us enough data to find the three unknown material specific parameters. Well layers of $In_{0.53}Ga_{0.47}As/InP$ SQW's were 20, 10, 7.5, and 5 nm wide, separated by 50-nm-wide barrier layers. Well layers of $In_{0.53}Ga_{0.47}As/In_{0.70}Ga_{0.30}As_{0.61}P_{0.39}$ SQW's were 20, 15, 10, and 5 nm wide, separated by 30-nm-wide barrier layers. Well layers of $GaAs/Al_{0.25}Ga_{0.75}As$ SQW's were 20, 15, 10, and 5 nm wide, separated by 50-nm-wide barrier layers. Cap and buffer layers were 200 nm wide in all samples. We controlled width and composition by growth conditions, which were checked by x-ray diffraction and transmission electron microscopy.

We annealed samples in a reactor tube of a liquid-phase epitaxy system; we placed an InP plate on $In_xGa_{1-x}As_yP_{1-y}$ samples and a GaAs plate on $Al_xGa_{1-x}As$ samples, and passed pure H_2 gas. We be-

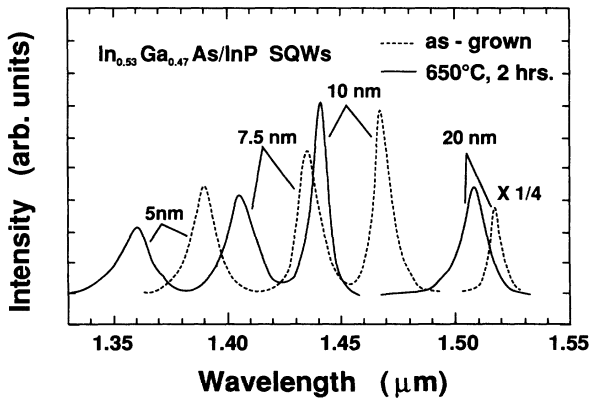

FIG. 1. Photoluminescence spectra of as-grown and annealed samples of $In_{0.53}Ga_{0.47}As/InP$ quantum wells 5, 7.5, 10, and 20 nm wide at 4.2 K. Annealing was for 2 h at 650 °C.

lieve that the semiconductor plates raise the vapor pressure of group-V elements (P or As) during annealing.

We measured photoluminescence spectra of these samples at 4.2 K before and after annealing by immersing samples in liquid helium. We excited luminescence with the 647.1-nm line of a Kr^+ ion laser and detected luminescence using a PbS detector. Figure 1 is an example of the measured photoluminescence spectra of $In_{0.53}Ga_{0.47}As/InP$ SQW's. The four peaks correspond to four quantum wells of different widths, and all of them shifted to a shorter wavelength after annealing. These peak shifts are caused by changes of quantum energy levels, which are sensitive to compositional profile.

IV. CALCULATION OF THE QUANTUM ENERGY SHIFT

We determined the three unknown parameters, interdiffusion coefficients, and the ratio of interfacial discontinuity by fitting quantum energy shifts calculated from our formula to measured ones. We used a numerical method to calculate quantum energies because the effective-mass equation[28] cannot be solved analytically in these cases.

The effective-mass equation is

$$\left[-\frac{\hbar^2}{2m_i}\frac{\partial^2}{\partial x^2}+V_i(x)+S_i(x)\right]\varphi_i(x)=E_i(x)\varphi_i(x), \quad i=e,\mathrm{HH},\mathrm{LH} \tag{19}$$

where $V_i(x)$ is the potential energy, $S_i(x)$ is the strain energy, E_i is the eigenenergy, and $\varphi_i(x)$ is the envelope wave function. Subscripts $i=e$, HH, and LH mean electron, heavy hole, and light hole, respectively. The potential energy $V_i(x)$ is calculated from the composition, which is shown as a function of x in our formula. The strain energy $S_i(x)$ is

$$S_c(x)=2a_c\frac{C_{11}-C_{12}}{C_{11}}\varepsilon(x) \tag{20}$$

and

$$S_v(x)=\left\{2a_v\frac{C_{11}-C_{12}}{C_{11}}\pm b\frac{C_{11}+2C_{12}}{C_{11}}\right\}\varepsilon(x), \tag{21}$$

where a_c and a_v are hydrostatic deformation potentials and b is shear deformation potential.[29–31] C_{11} and C_{12} are elastic stiffness. $\varepsilon(x)$ is misfit strain. The plus and the minus correspond to light-hole band and heavy-hole band, respectively.

We used the Runge-Kutta method suggested by Sakurai[32] to solve the effective-mass equations. We computed the envelope function numerically, with the boundary conditions that both $\varphi_i(x)$ and $1/m_i\partial\varphi_i(x)/\partial x$ are continuous at the interface, and we determined eigenenergies for both the conduction band and the valence band. We calculated total energy shifts as the sum of the energy shift in the two bands.

We used the following parameters to calculate the quantum energy levels $In_{1-x}Ga_xAs_yP_{1-y}/InP$ quantum wells: effective mass $m_e=0.041m_0$, $m_{HH}=0.50m_0$, and $m_{LH}=0.052m_0$ in an $In_{0.53}Ga_{0.47}As$ well layer; $m_e=0.08m_0$ and $m_{HH}=0.56m_0$ in an InP barrier layer; $m_e=0.044m_0$ and $m_{HH}=0.49m_0$ in an $In_{0.70}Ga_{0.30}As_{0.61}P_{0.39}$ barrier layer; elastic stiffness $C_{11}=1.016\times10^{11}$ dyn/cm^2 and $C_{12}=0.509\times10^{11}$ dyn/cm^2;[33] and distribution ratio of conduction-band offset $\Delta E_c=0.4\Delta E_g$.[34] We used the hydrostatic deformation potentials $a_c=a_v=-3.94$ eV and the shear deformation potential $b=-1.7$ eV.[35] We assumed that the hydrostatic deformation potential was distributed evenly between the conduction and the valence band and neglected the compositional dependence of these three deformation potentials. Since the compositional dependence of energy gap at 4.2 K is not reported to our knowledge, we used the compositional dependence at 295 K:[36]

$$E_g^{295\ \mathrm{K}}(x,y)=1.35+0.672x-1.091y+0.758x^2+0.101y^2+0.111xy-0.580x^2y-0.159xy^2+0.268x^2y^2. \tag{22}$$

We believe that this is a good approximation when calculating shifts of quantum energies since band offset does not depend on temperature.

We used the following material parameters when calculating quantum energy levels in $GaAs/Al_xGa_{1-x}As$ quantum wells: effective mass $m_e=0.067m_0$ and $m_{HH}=0.42m_0$ in a GaAs well layer, $m_e=0.088m_0$ and $m_{HH}=0.53m_0$ in an $Al_{0.25}Ga_{0.75}As$ barrier layer, and distribution ratio of conduction-band offset $\Delta E_c=0.65\Delta E_g$.[14] Strain energy is negligible in this material. For the same reason as with an $In_{1-x}Ga_xAs_yP_{1-y}$ system, we used the compositional dependence of the energy gap of $Al_xGa_{1-x}As$ at 300 K:[37]

$$E_g^{300\ \mathrm{K}}(x)=1.424+1.247x \tag{23}$$

and calculated shifts of quantum energies.

V. THE INTERDIFFUSION PROCESS IN QUANTUM WELLS

We compare the measured and the calculated dependence of quantum energy shifts on well layer width for various annealing times in $In_{0.53}Ga_{0.47}As/InP$ and in $GaAs/Al_{0.25}Ga_{0.75}As$ quantum wells [Figs. 2(a) and 2(b)]. Solid lines are shifts calculated using our formula. The dependence of energy shifts is different for each type of quantum well, and calculated shifts and measured shifts agree closely for both materials. In $In_{0.53}Ga_{0.47}As/InP$ quantum wells [Fig. 2(a)], the energy shift increased gradually in 20-nm-wide well layers, and in the narrower well layers, the shift increased rapidly up to 2 h and then saturated. In $GaAs/Al_{0.25}Ga_{0.75}As$ quantum wells [Fig. 2(b)], the energy in the 20-nm-wide well layer was almost constant, and in the narrower well layers, the energy shift increased and did not saturate. Our formula explained each of these characteristics with a set of parameters, that is, interdiffusion coefficients in each layer and inter-

facial distribution ratio. This result is consistent with our fundamental assumption that the three parameters can be regarded as constant during interdiffusion. Note that this assumption for interdiffusion coefficient is equivalent to assuming that the coefficient depends very little on the composition of group-V atoms. Our result suggests that the assumption is valid, at least under our experimental conditions.

We measured the dependence of quantum energy shifts on well layer width at various annealing temperatures (Fig. 3) for (a) $In_{0.53}Ga_{0.47}As/InP$ quantum wells, (b) $In_{0.53}Ga_{0.47}As/In_{0.70}Ga_{0.30}As_{0.61}P_{0.39}$ quantum wells, and (c) $GaAs/Al_{0.25}Ga_{0.75}As$ quantum wells. The solid lines are the calculated shifts and agree well with the measured shifts in all the figures. Tables I and II list calculated interdiffusion coefficients and distribution ratios for $In_{1-x}Ga_xAs_yP_{1-y}/InP$ and $GaAs/Al_{0.25}Ga_{0.75}As$ quantum wells. We found that interdiffusion coefficients in $In_{0.53}Ga_{0.47}As$ layers were common to quantum wells

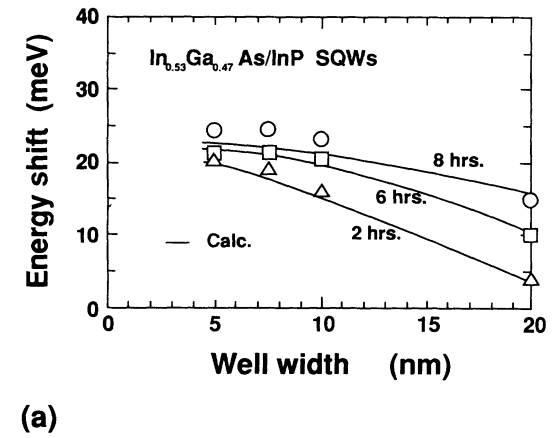

(a)

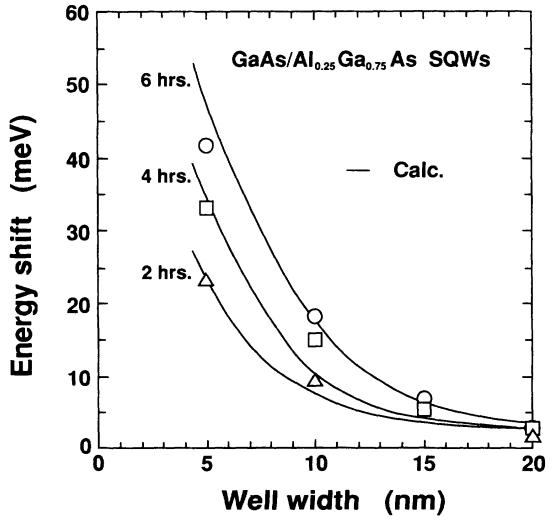

(b)

FIG. 2. Quantum energy shifts as a function of well width. (a) $In_{0.53}Ga_{0.47}As/InP$ quantum wells after annealing at 650 °C for 2, 6, and 8 h. (b) $GaAs/Al_{0.25}Ga_{0.75}As$ quantum wells after annealing at 825 °C for 2, 4, and 6 h. Symbols are measured results and solid lines are calculated results.

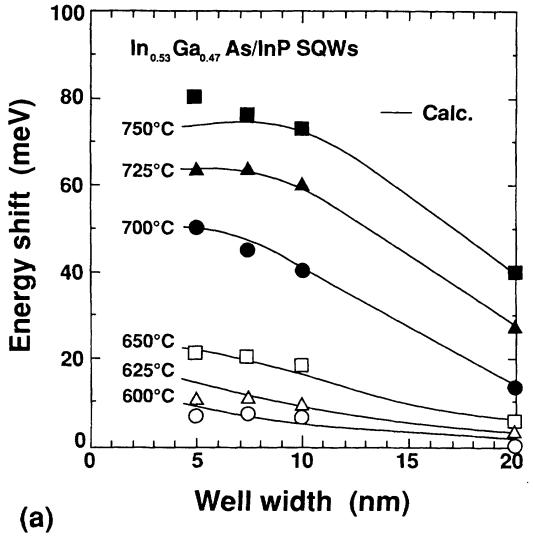

(a)

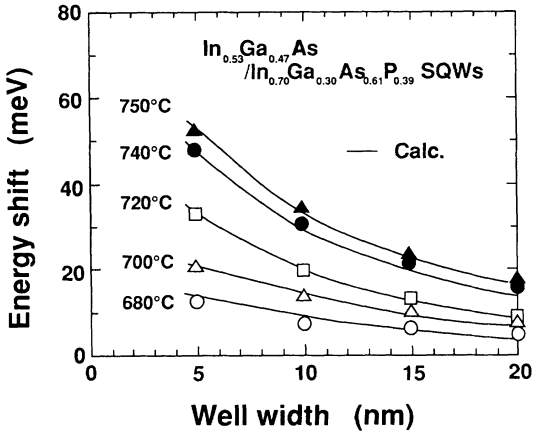

(b)

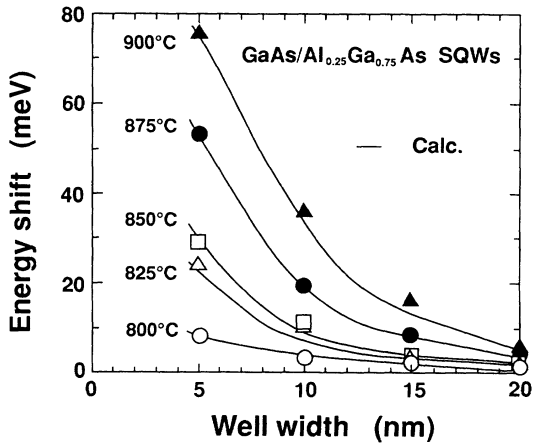

(c)

FIG. 3. Quantum energy shifts as a function of well width. (a) $In_{0.53}Ga_{0.47}As/InP$ quantum wells after annealing at 600 °C–750 °C for 2 h. (b) $In_{0.53}Ga_{0.47}As/In_{0.70}Ga_{0.30}As_{0.61}P_{0.39}$ quantum wells after annealing at 680 °C–750 °C for 2 h. (c) $GaAs/Al_{0.25}Ga_{0.75}As$ quantum wells after annealing at 800 °C and 900 °C for 2 h. Symbols are measured results and solid lines are calculated results.

TABLE I. Interdiffusion coefficients and distribution ratios of $In_{0.53}Ga_{0.47}As/InP$ and $In_{0.53}Ga_{0.47}As/In_{0.70}Ga_{0.30}As_{0.61}P_{0.39}$ quantum wells.

	$In_{0.53}Ga_{0.47}As/InP$			$In_{0.53}Ga_{0.47}As/In_{0.70}Ga_{0.30}As_{0.61}P_{0.39}$		
T (°C)	D_{InGaAs} (cm^2/s)	D_{InP} (cm^2/s)	k	D_{InGaAs} (cm^2/s)	$D_{InGaAsP}$ (cm^2/s)	k
600	1.7×10^{-17}	4.3×10^{-21}	40			
625	2.0×10^{-17}	2.0×10^{-20}	35			
650	2.1×10^{-17}	2.1×10^{-19}	30	2.6×10^{-17}	5.1×10^{-20}	2
700	2.8×10^{-17}	5.6×10^{-17}	17	2.8×10^{-17}	1.4×10^{-19}	2
720				3.5×10^{-17}	2.3×10^{-19}	1
725	3.8×10^{-17}	3.8×10^{-15}	13			
740				3.5×10^{-17}	4.3×10^{-19}	1
750	4.7×10^{-17}	4.7×10^{-14}	11	3.9×10^{-17}	5.5×10^{-19}	1

having different barrier layers. The distribution ratio k decreased as the annealing temperature increased in $In_{0.53}Ga_{0.47}As/InP$ quantum wells. The parameters in Table I explain why the tendency in Fig. 3(b) is between Figs. 3(a) and 3(c). Interdiffusion coefficients of $In_{0.53}Ga_{0.47}As/In_{0.70}Ga_{0.30}As_{0.61}P_{0.39}$ quantum wells were quite different between layers, which is a characteristic of $In_{0.53}Ga_{0.47}As/InP$, and interfacial discontinuity is small, which is a characteristic of $GaAs/Al_{0.25}Ga_{0.75}As$. The parameters in Table II suggest that Chang and Koma's model is applicable to $GaAs/Al_xGa_{1-x}As$ quantum wells. We confirmed that interdiffusion coefficients were common to both layers and that distribution ratios were 1 at all the annealing temperatures we tried for $GaAs/Al_{0.25}Ga_{0.75}As$ quantum wells.

We calculated interdiffusion profiles of $In_{0.53}Ga_{0.47}As/InP$ and $GaAs/Al_{0.25}Ga_{0.75}As$ quantum wells [Figs. 4(a) and 4(b)]. Figure 4(a) explains the results found by Nakashima *et al.*[15] and Fujii *et al.*[16] These profiles help us understand the characteristics of energy shift in two types of quantum well. In $In_{0.53}Ga_{0.47}As/InP$ quantum wells [Fig. 4(a)], there is a large interfacial discontinuity, which starts as the distribution ratio. The distribution ratio limits the increase of phosphorus composition in the well layer. Because of this compositional limitation, the shift of quantum energy saturates. By high velocity of interdiffusion (see Table I), interdiffusion easily advances to the center of the well layer. Quantum energies therefore shift even in a wide well layer. Distribution ratios were independent of well layer width, so saturation and shift occur earlier in narrower well layers. With $GaAs/Al_{0.25}Ga_{0.75}As$ quantum wells [Fig. 4(b)], the distribution ratio was 1, so energy shifts did not saturate and increased gradually.

TABLE II. Interdiffusion coefficients and distribution ratios of $GaAs/Al_{0.25}Ga_{0.75}As$ quantum wells. Interdiffusion coefficients of GaAs and $Al_{0.25}Ga_{0.75}As$ layers were equal.

	$GaAs/Al_{0.25}Ga_{0.75}As$	
T (°C)	D (cm^2/s)	k
800	2.2×10^{-19}	1
825	6.9×10^{-19}	1
850	1.1×10^{-18}	1
875	2.3×10^{-18}	1
900	4.0×10^{-18}	1

We made Arrhenius plots of interdiffusion coefficients in $In_{1-x}Ga_xAs_yP_{1-y}/InP$ and $GaAs/Al_xGa_{1-x}As$ quantum wells [Figs. 5(a) and 5(b)]. The solid lines are for an Arrhenius expression with a single activation energy. We found that activation energy was 0.5 eV in an $In_{0.53}Ga_{0.47}As$ layer, 2.0 eV in an $In_{0.70}Ga_{0.30}As_{0.61}P_{0.39}$ layer, and 8.4 eV in an InP layer [Fig. 5(a)]. The activation energy in InP was larger than the energy of self-diffusion of phosphorus atoms in InP, which has been measured as 5.65 eV.[38] We suggest that one reason for this discrepancy is lattice distortion adding excess energy to the activation energy. We cannot compare activation energies in $In_{0.53}Ga_{0.47}As$ and $In_{0.70}Ga_{0.30}As_{0.61}P_{0.39}$ layers with other values for a lack of reported data. We found an interdiffusion activation energy in $GaAs/Al_{0.25}Ga_{0.75}As$ quantum wells of 2.8 eV. We superimposed previous reported data in Fig. 5(b). We believe that the discrepancy between our value and others is caused by a difference in crystal quality. Chang and Koma found an interdiffusion activation energy in $Al_{0.25}Ga_{0.75}As$ of 4.1 eV.[1] They speculated that the disagreement between their activation energy and the Ga vacancy, which was 2.1 eV,[39] was due to an As vacancy via the formation of a divacancy.[40] Our activation energy was closer to Ga vacancy than Chang and Koma's, so it is possible that our samples had less As vacancy than their sample. This would also explain why our interdiffusion coefficients were lower than theirs. Guido *et al.* studied the influence of vacancy concentration on interdiffusion.[12] The smallest activation energy of their various samples was 3.4 eV. Their results were very similar to ours, though their activation energy was different.

We also reached some conclusions about the characteristics of interdiffusion of group-V atoms in $In_{1-x}Ga_xAs_yP_{1-y}$ materials. We assume that interfacial compositional discontinuity is related to lattice distortion, which is first generated at the interface during interdiffusion. If there is no interfacial discontinuity, the greater the difference in initial composition of group-V atoms between well and barrier layers, the greater the lattice distortion produced by interdiffusion. In Table I distribution ratios of $In_{0.53}Ga_{0.47}As/InP$ quantum wells were larger than those of

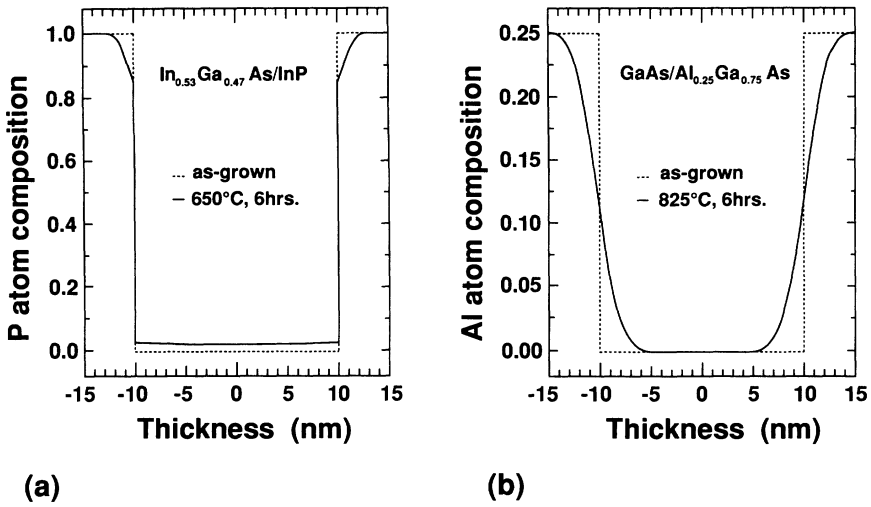

FIG. 4. (a) Calculated phosphorus composition profile in an $In_{0.53}Ga_{0.47}As/InP$ quantum well 20 nm wide after annealing at 650 °C for 6 h. (b) Calculated aluminum composition profile in a $GaAs/Al_{0.25}Ga_{0.75}As$ quantum well 20 nm wide after annealing at 825 °C for 6 h.

$In_{0.53}Ga_{0.47}As/In_{0.70}Ga_{0.30}As_{0.61}P_{0.39}$ quantum wells. In Table II the ratios obtained a value of unity in $GaAs/Al_xGa_{1-x}As$ quantum wells, where interfacial lattice distortion is negligible. This shows that the distribution ratio was larger at the interface where the greater lattice distortion was expected. We can also see from Table I that the distribution ratio dropped as the annealing temperature increased. These results support the assumption that compositional discontinuity starts by a thermodynamic potential barrier related to lattice distortion. Yu *et al.* reported that lattice mismatch was avoided when both group-III atoms and group-V atoms interdiffuse. They speculated that the avoidance was because interdiffusion producing lattice distortion requires excess energy.[41] Considering that the stress energy will follow the compositional profiles in layers, the ratio k is expected to vary versus time. We suppose that the annealing time in our experiment is not so long that the effect of change in the compositional profile could not be observed in this work.

Even though we neglected the Smigelskas-Kirkendall effect, our model accurately explained quantum energy shifts due to interdiffusion. This suggests that the Smigelskas-Kirkendall effect was negligible in our samples. We assume that this result is also related to lattice distortion adding excess energy to interdiffusion activation energy. When group-III atoms do not move, as in our experiment, motion of the interface of group-V atoms must produce quite a large lattice distortion between the interface of group-III atoms and that of group-V atoms.

VI. CONCLUSION

We presented a formula that describes interdiffusion profiles of quantum wells. We looked at the interdiffusion process in quantum wells composed of $In_xGa_{1-x}As_yP_{1-y}$ and $Al_xGa_{1-x}As$ alloy semiconductors and showed the accuracy of our formula. We derived our formula by solving diffusion equations assuming that interdiffusion coefficients differ between layers and that there is interfacial discontinuity in the composition of interdiffused species. The formula includes the

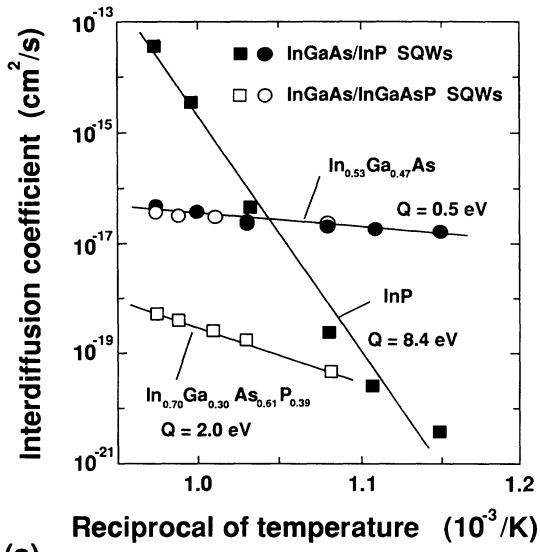

FIG. 5. Interdiffusion coefficients as a function of the reciprocal of annealing temperature. (a) $In_xGa_{1-x}As_yP_{1-y}$ quantum wells. (b) $GaAs/Al_{0.25}Ga_{0.75}As$ quantum wells. Results of previous research are shown in (b).

penetration of interdiffusion between alternate layers, which is common in quantum wells. We applied the formula to analyzing the dependence of a quantum energy shift on annealing time, annealing temperature, and well layer width in lattice-matched $In_xGa_{1-x}As_yP_{1-y}/InP$ and $GaAs/Al_xGa_{1-x}As$ quantum wells. Our formula correctly predicted the dependence and clarified the differences between interdiffusion processes in these two materials.

ACKNOWLEDGMENTS

The authors would like to thank S. Yamakoshi, T. Tanahashi, and T. Fujii for their helpful advice and N. Okazaki and O. Aoki for their technical assistance. K. M. would like to thank Sachiko Mukai for her encouragement during the course of this work.

APPENDIX

We rearranged Eqs. (4)–(7) to give the conventional solution. C_2 can be expressed by a Maclaurin expression using the value at $x=L$:

$$C_2(x',t)=C_2(x',t)|_0+x'\left.\frac{\partial C_2(x',t)}{\partial x'}\right|_0+\frac{x'^2}{2!}\left.\frac{\partial^2 C_2(x',t)}{\partial x'^2}\right|_0+\cdots=\sum_{n=0}^{\infty}\frac{x'^n}{n!}\left.\frac{\partial^n C_2(x',t)}{\partial x'^n}\right|_0, \tag{A1}$$

where $x'=x-L$. From Eqs. (1) and (2), we get

$$\frac{\partial^n C_1(x',t)}{\partial t^n}=D_1^n\frac{\partial^{2n}C_1(x',t)}{\partial x'^{2n}}, \tag{A2}$$

$$\frac{\partial^n C_2(x',t)}{\partial t^n}=D_2^n\frac{\partial^{2n}C_2(x',t)}{\partial x'^{2n}}. \tag{A3}$$

We differentiate Eqs. (4) and (6) by t and substitute them into Eq. (A2) and get

$$D_1^n\left.\frac{\partial^{2n}C_1(x',t)}{\partial x'^{2n}}\right|_0=kD_2^n\left.\frac{\partial^{2n}C_2(x',t)}{\partial x'^{2n}}\right|_0, \tag{A4}$$

$$D_1^{n+1}\left.\frac{\partial^{2n+1}C_1(x',t)}{\partial x'^{2n+1}}\right|_0=kD_2^{n+1}\left.\frac{\partial^{2n+1}C_2(x',t)}{\partial x'^{2n+1}}\right|_0. \tag{A5}$$

We substitute Eqs. (A2)–(A5) into Eq. (A1):

$$C_2(x',t)=\frac{1}{2}\left[\frac{1}{k}+a\right]\sum_{n=0}^{\infty}\frac{1}{n!}(ax')^n\left.\frac{\partial^n C_1(x',t)}{\partial x'^n}\right|_0+\frac{1}{2}\left[\frac{1}{k}-a\right]\sum_{n=0}^{\infty}\frac{1}{n!}(-ax')^n\left.\frac{\partial^n C_1(x',t)}{\partial x'^n}\right|_0, \tag{A6}$$

where $a=\sqrt{D_1/D_2}$. We then get the condition

$$C_2(x-L,t)=\frac{1}{2}\left[\frac{1}{k}+a\right]C_1[a(x-L,t)]+\frac{1}{2}\left[\frac{1}{k}-a\right]C_1[-a(x-L,t)]. \tag{A7}$$

Using the same solution as above, we get

$$C_1(x-L,t)=\frac{1}{2}\left[k+\frac{1}{a}\right]C_2\left[\frac{1}{a}(x-L,t)\right]+\frac{1}{2}\left[k-\frac{1}{a}\right]C_2\left[-\frac{1}{a}(x-L,t)\right]. \tag{A8}$$

At $x=-L$, in the same way as for $C_1(x,t)$ and $C_2(x,t)$ above, we get

$$C_2(x+L,t)=\frac{1}{2}\left[\frac{1}{k}+a\right]C_3[a(x+L,t)]+\frac{1}{2}\left[\frac{1}{k}-a\right]C_3[-a(x+L,t)] \tag{A9}$$

and

$$C_3(x+L,t)=\frac{1}{2}\left[k+\frac{1}{a}\right]C_2\left[\frac{1}{a}(x+L,t)\right]+\frac{1}{2}\left[k-\frac{1}{a}\right]C_2\left[-\frac{1}{a}(x+L,t)\right]. \tag{A10}$$

Note that Eqs. (A7)–(A10) are sufficient conditions for Eqs. (4)–(7).

The solution must satisfy diffusion equations Eqs. (1)–(3), boundary conditions Eqs. (A7)–(A10), and the initial condition Eq. (8). If we consider only two layers separated by the boundary at $x=L$, the solutions are[25]

$$C_1(x,t)=\frac{1}{2\sqrt{\pi D_1 t}}\left\{\exp\left[-\frac{(x-\xi)^2}{4D_1t}\right]-\frac{1-ak}{1+ak}\exp\left[-\frac{(x-2L+\xi)^2}{4D_1t}\right]\right\},\quad x\geq L \tag{A11}$$

$$C_2(x,t)=\frac{1}{2\sqrt{\pi D_1 t}}\frac{2a}{1+ak}\exp\left[-\frac{\left[x-L+\frac{L}{a}-\frac{\xi}{a}\right]^2}{4D_2t}\right],\quad |x|<L. \tag{A12}$$

These are normalized. Considering the boundary at $x=-L$ [Eqs. (A9) and (A10)] and the initial condition [Eq. (8)], Eq. (A12) has to be transformed to

$$C_2(x,t)=\frac{1}{2\sqrt{\pi D_1 t}}\left\{\frac{2a}{1+ak}\exp\left[-\frac{\left[x-L+\frac{L}{a}-\frac{\xi}{a}\right]^2}{4D_2 t}\right]+\frac{2a(1-ak)}{(1+ak)^2}\exp\left[-\frac{\left[x+3L-\frac{L}{a}+\frac{\xi}{a}\right]^2}{4D_2 t}\right]\right\}, \quad |x|<L \tag{A13}$$

and then

$$C_3(x,t)=\frac{1}{2\sqrt{\pi D_1 t}}\frac{4ak}{(1+ak)^2}\exp\left[-\frac{(x+2L-2aL-\xi)^2}{4D_1 t}\right], \quad x\le -L\ . \tag{A14}$$

Due to the added second term of Eq. (A13), Eq. (A11) has to be transformed to

$$C_1(x,t)=\frac{1}{2\sqrt{\pi D_1 t}}\left\{\exp\left[-\frac{(x-\xi)^2}{4D_1 t}\right]-\frac{1-ak}{1+ak}\exp\left[-\frac{(x-2L+\xi)^2}{4D_1 t}\right]+\frac{1-ak}{1+ak}\exp\left[-\frac{(x-2L+4aL+\xi)^2}{4D_1 t}\right]-\left[\frac{1-ak}{1+ak}\right]^2\exp\left[-\frac{(x-4aL-\xi)^2}{4D_1 t}\right]\right\}, \quad x\ge L\ . \tag{A15}$$

Equation (A15) satisfies the diffusion equations and the boundary conditions, but not the initial conditions. The last term of Eq. (A15) shows that there is a diffusion source at $x=4aL+\xi$, which contradicts the single source in Eq. (8). In order to cancel this last term, we introduce a negative source at $x=4aL+\xi$, which has the same absolute value as the last term of Eq. (A15). This imaginary source needs additional terms in regions $x\ge L$, $|x|<L$, and $x\le -L$ to satisfy the boundary conditions Eqs. (A7)–(A10). This, however, also produces a diffusion source in $x\ge L$. We finally found that solutions which satisfy all conditions are infinite series.

[1] L. L. Chang and Koma, Appl. Phys. Lett. **29**, 138 (1976).

[2] W. D. Laidig, N. Holonyak, Jr., M. D. Camras, K. Hess, J. J. Coleman, P. D. Dapkus, and J. Bardeen, Appl. Phys. Lett. **38**, 776 (1981).

[3] M. Kawabe, N. Matsuura, N. Shimizu, F. Hasegawa, and Y. Ninnichi, Jpn. J. Appl. Phys. **23**, L623 (1984).

[4] K. Meehan, N. Holonyak, Jr., J. M. Brown, M. A. Nixon, and P. Gavrilovic, Appl. Phys. Lett. **45**, 549 (1984).

[5] E. V. K. Rao, H. Thibiergr, F. Brillouet, F. Alexandre, and R. Azoulay, Appl. Phys. Lett. **46**, 867 (1985).

[6] R. L. Thornton, R. D. Burnham, T. L. Paoli, N. Holonyak, Jr., and D. G. Deppe, Appl. Phys. Lett. **48**, 7 (1986).

[7] R. L. Thornton, R. D. Burnham, T. L. Paoli, N. Holonyak, Jr., and D. G. Deppe, Appl. Phys. Lett. **47**, 1239 (1985).

[8] T. Fukuzawa, S. Semura, H. Saito, T. Ohta, Y. Uchida, and H. Nakashima, Appl. Phys. Lett. **45**, 1 (1984).

[9] J. Cibert, P. M. Petroff, D. J. Werder, S. J. Pearton, A. C. Gossard, and J. H. English, Appl. Phys. Lett. **49**, 223 (1986).

[10] D. G. Deppe, L. J. Guido, N. Holonyak, Jr., K. C. Hsieh, R. D. Burnham, R. L. Thornton, and T. L. Paoli, Appl. Phys. Lett. **49**, 510 (1986).

[11] J. Cibert, P. M. Petroff, G. J. Dolan, S. J. Pearton, A. C. Gossard, and J. H. English, Appl. Phys. Lett. **49**, 1275 (1986).

[12] L. J. Guido, N. Holonyak, Jr., K. C. Hsieh, R. W. Kaliski, W. E. Plano, R. D. Burnham, R. L. Thornton, J. E. Epler, and T. L. Paoli, J. Appl. Phys. **61**, 1372 (1987).

[13] M. D. Camras, T. L. Paoli, and C. Linstrom, J. Appl. Phys. **54**, 5637 (1983).

[14] H. Leier, H. Rothfritz, and Forchel, J. Appl. Phys. **95**, 277 (1989).

[15] K. Nakashima, Y. Kawaguchi, Y. Kawamura, H. Asahi, and Y. Imamura, Jpn. J. Appl. Phys. **26**, L1620 (1987).

[16] T. Fujii, N. Sugawara, S. Yamazaki, and K. Nakajima, J. Cryst. Growth **105**, 348 (1990).

[17] B. Tell, B. C. Johnson, J. L. Zyskind, J. M. Brown, J. W. Sulhoff, K. F. Brown-Goebeler, B. I. Miller, and U. Koren, Appl. Phys. Lett. **52**, 1428 (1988).

[18] M. Razeghi, O. Acher, and F. Launay, Semicond. Sci. Technol. **2**, 793 (1987).

[19] K. Nakashima, Y. Kawaguchi, Y. Kawamura, and Y. Imamura, Appl. Phys. Lett. **52**, 1383 (1988).

[20] S. A. Schwarz, P. Mei, T. Venkatesan, R. Bhat, D. M. Hwang, C. L. Schwartz, M. Koza, L. Nazar, and B. J. Skromme, Appl. Phys. Lett. **53**, 1051 (1988).

[21] H. Sumida, H. Asahi, S. J. Yu, K. Asami, and S. Gonda, Appl. Phys. Lett. **54**, 520 (1989).

[22] H. Ribot, K. W. Lee, R. J. Simes, R. H. Yan, and L. A. Coldren, Appl. Phys. Lett. **55**, 672 (1989).

[23] E. S. Koteles, A. N. M. M. Choudhury, A. Levy, B. Elman, P. Melman, M. A. Koza, and R. Bhat, in *Advanced III-V Compound Semiconductor Growth, Processing and Devices,* edited by S. J. Pearton, D. K. Sadana, and J. M. Zavada, MRS Symposia Proceedings No. 240 (Materials Research Society, Pittsburgh, 1991), p. 171.

[24] R. M. Flemming, D. B. McWhan, A. C. Gossard, W. Wiegmann, and R. A. Logan, J. Appl. Phys. **51**, 357 (1980).

[25] W. Jost, *Diffusion* (Academic, New York, 1960), p. 68.

[26] R. Smoluchowski, Phys. Rev. **62**, 539 (1942).

[27] H. E. Cook and J. E. Hilliard, J. Appl. Phys. **40**, 2191 (1969).

[28] H. Haken, *Quantenfeldtheorie des Festkorpers* (Teubner, Stuttgart, 1973).

[29] G. E. Pikus and G. L. Bir, Fiz. Tverd. Tela (Leningrad) **1**, 154

(1959) [Sov. Phys. Solid State **1**, 136 (1959)].
[30]G. E. Pikus and G. L. Bir, Fiz. Tverd. Tela (Leningrad) **1**, 1642 (1959) [Sov. Phys. Solid State **1**, 1502 (1960)].
[31]A. Gavini and M. Cardona, Phys. Rev. B **1**, 672 (1970).
[32]K. Sakurai, *Introduction to Quantum Mechanics by Personal Computer* (Shokabo, Tokyo, 1989) [in Japanese].
[33]M. C. Joncour, J. L. Benchimol, J. Burgeat, and M. Quillec, J. Phys. (Paris) Colloq. **5**, 3 (1982).
[34]S. R. Forest, P. H. Schmidt, R. B. Wilson, and M. L. Kaplan, Appl. Phys. Lett. **45**, 1199 (1984).
[35]C. P. Kuo, S. K. Vong, R. M. Cohen, and G. B. Stringfellow, J. Appl. Phys. **57**, 5428 (1985).
[36]Y. Suematsu, *Semiconductor Laser and OEIC* (Orhm Inc., Tokyo, 1984), p. 70 [in Japanese].
[37]H. C. Casey, Jr., J. Appl. Phys. **49**, 3684 (1978).
[38]B. Goldstein, Phys. Rev. **121**, 1305 (1961).
[39]S. Y. Chiang and G. L. Pearson, J. Appl. Phys. **46**, 2986 (1975).
[40]D. L. Kendal, in *Semicoductors and Semimetals* (Academic, New York, 1968), Vol. 4, p. 163.
[41]S. J. Yu, H. Asahi, S. Emura, S. Gonda, and K. Nakashima, J. Appl. Phys. **70**, 204 (1991).